Solubility of water in hydrogen at high pressures

A molecular simulation study

Rahbari, Ahmadreza; Brenkman, Jeroen; Hens, Remco; Ramdin, Mahinder; Van Den Broeke, Leo J.P.; Schoon, Rogier; Henkes, Ruud; Moultos, Othonas A.; Vlugt, Thijs J.H.

Important note
To cite this publication, please use the final published version (if applicable).
Please check the document version above.

Article

Solubility of Water in Hydrogen at High Pressures: A Molecular Simulation Study

Ahmadreza Rahbari,[†] Jeroen Brenkman,[‡] Remco Hens,[†] Mahinder Ramdin,[†] Leo J. P. van den Broeke,[†] Rogier Schoon,[‡] Ruud Henkes,[‡] Othonas A. Moultos,[†] and Thijs J. H. Vlugt*,[†]

[†]Engineering Thermodynamics, Process & Energy Department, Faculty of Mechanical, Maritime and Materials Engineering, Delft University of Technology, Leeghwaterstraat 39, 2628CB, Delft, The Netherlands

[‡]Shell Global Solutions International, PO Box 38000, 1030BN, Amsterdam, The Netherlands

S *Supporting Information*

ABSTRACT: Hydrogen is one of the most popular alternatives for energy storage. Because of its low volumetric energy density, hydrogen should be compressed for practical storage and transportation purposes. Recently, electrochemical hydrogen compressors (EHCs) have been developed that are capable of compressing hydrogen up to P = 1000 bar, and have the potential of reducing compression costs to 3 kWh/kg. As EHC compressed hydrogen is saturated with water, the maximum water content in gaseous hydrogen should meet the fuel requirements issued by the International Organization for Standardization (ISO) when refuelling fuel cell electric vehicles. The ISO 14687−2:2012 standard has limited the water concentration in hydrogen gas to 5 μmol water per mol

hydrogen fuel mixture. Knowledge on the vapor liquid equilibrium of H_2O-H_2 mixtures is crucial for designing a method to remove H_2O from compressed H_2. To the best of our knowledge, the only experimental high pressure data (P > 300 bar) for the H_2O-H_2 phase coexistence is from 1927 [*J. Am. Chem. Soc.*, **1927**, *49*, 65−78]. In this paper, we have used molecular simulation and thermodynamic modeling to study the phase coexistence of the H_2O-H_2 system for temperatures between T = 283 K and T = 423 K and pressures between P = 10 bar and P = 1000 bar. It is shown that the Peng-Robinson equation of state and the Soave Redlich-Kwong equation of state with van der Waals mixing rules fail to accurately predict the equilibrium coexistence compositions of the liquid and gas phase, with or without fitted binary interaction parameters. We have shown that the solubility of water in compressed hydrogen is adequately predicted using force-field-based molecular simulations. The modeling of phase coexistence of H_2O-H_2 mixtures will be improved by using polarizable models for water. In the Supporting Information, we present a detailed overview of available experimental vapor−liquid equilibrium and solubility data for the H_2O-H_2 system at high pressures.
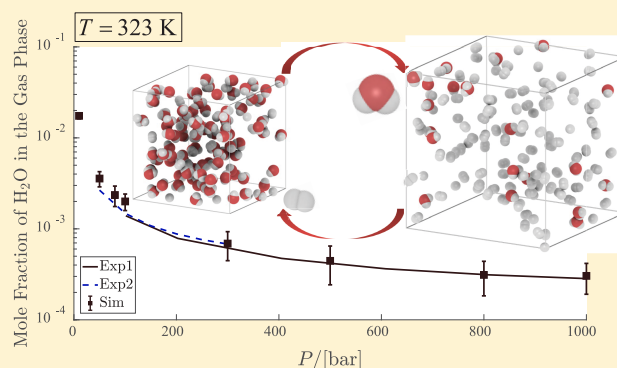
1. INTRODUCTION

The world population is expected to grow rapidly, from 7.6 billion currently, to about 9.8 billion in 2050.[1] Due to increasing prosperity, the worldwide consumption of energy per individual will also increase. Even in the current modern world, several billion people still do not have access to basic needs, such as clean water, sanitation, nutrition, health care, and education.[2] These are all examples of the Sustainable Development Goals, adopted by all United Nations Member States in 2015.[2] Access to energy is a key enabler to reach these basic needs. The worldwide energy demand is therefore expected to increase by 40% by 2040.[3] At the same time, CO_2 emissions need to be reduced to reach the goals of the Paris agreement.[4] Roughly, 80% of the total primary energy supply is currently produced by fossil fuels, such as coal, oil, and natural gas.[3] To reach the goals of the Paris agreement, attempts have

been made to replace fossil fuels with renewable alternatives such as wind and solar (PV) energy. Current expectations are that by 2040, 40% of the total generated electricity will be from renewable energy sources.[3]

Unlike fossil fuels, energy production from intermittent renewable sources, including wind power and solar energy, critically depend on the availability of these sources leading to an uncontrollable energy output.[5] For direct integration to the power grid, uncontrollable availability of intermittent renewable energy sources within 10% of the installed capacity is acceptable without major technical problems.[5] However, large scale integration of intermittent energy sources above this limit

is expected to cause frequent mismatches between the supply and demand of energy. To avoid this, the integration of energy storage technologies is proposed as one of the promising solutions for stable and flexible supply of electricity.[6,7] Different types of technologies have been developed for electrical energy storage including: hydrostorage, flywheels, batteries, and hydrogen produced by electrolysis, etc.[5,6,8,9] One of the most popular alternatives for energy storage is hydrogen.[8] Hydrogen has the advantage that it can be stored for long periods and converted to electricity without pollution.[10] Hydrogen has a broad span of applications, such as fuel cells, fuel for heating, transportation, or even as a raw material for the chemical industry.[5,10,11] Since hydrogen has a very low density at standard conditions, it has a very low volumetric energy density. For practical storage and transportation purposes, the density of hydrogen must be increased significantly.[12] The density of hydrogen can be increased by compression, cooling, or a combination of both, depending on the scale and application.[12] One of the emerging applications for hydrogen is found in sustainable transportation.[10] In fuel cell electric vehicles (FCEV), hydrogen is stored in compressed form in pressurized cylinders at $P = 350$ bar or $P = 700$ bar.[12] In practice, a passenger car needs a tank capacity of ca. 100 to 150 L to store 4 to 6 kg of hydrogen, which provides a range of approximately 500 km.[12] High pressure storage tanks with pressures of at least $P = 875$ bar[12,13] are installed at refuelling stations, to fuel a vehicle within the target time of 3 to 5 min.[12] Conventional compressor types that are currently used are piston, compressed air, diaphragm, or ionic compressors, depending mainly on the capacity of the refuelling station.[12] The conventional compressor requires on average 6 kWh/kg of energy to compress hydrogen from 10 to 400 bar.[13]

An alternative compressor is the electrochemical hydrogen compressor (EHC). HyET Hydrogen BV[14] has developed an EHC that works with pressures up to 1000 bar, and has the potential of bringing compression costs down to 3 kWh/kg.[13] The working principle of an EHC operation is similar to a proton exchange membrane (PEM) fuel cell.[15] A single EHC stack consists of a low pressure and a high pressure side, separated by a membrane that is only permeable for hydrogen protons, and not for molecules. The membrane is positioned between two platinum catalysts containing electrodes. Once a potential difference is applied over the electrodes, a hydrogen molecule splits into two protons. The protons then travel through the membrane where conversion to hydrogen molecules takes place at elevated pressure.[15] In the EHC, the proton transfer through the membrane is enabled by water. The EHC has several advantages compared to traditional technologies:[13,16−18] (1) The EHC has a higher efficiency, especially at high compression ratios.[19] In theory, the compression ratio using EHC can go to infinity, from an electrochemical perspective. The mechanical strength and back diffusion losses are the main limitations for higher pressure ratios for the EHC.[19] (2) Due to the highly selective membrane that only allows the permeation of protons, contaminants are prevented from passing the membrane.[19] This means that the EHC performs both as a compressor and a purifier of hydrogen gas.[19] (3) The compressor has no moving parts, resulting in lower maintenance costs and making lubricants, which may contaminate the compressed hydrogen, redundant. (4) The EHC operates silently, since it has no rotating parts. This makes the EHC suitable for locations such

as refuelling stations, where acoustical emission is a constraint. (5) The EHC is a compact device that is well suited to scale up.[19] Disadvantages of the EHC are similar to those of fuel cells, mainly high material costs. For instance, the platinum catalyst which is required to resist the corrosive environments in the compressor, is very expensive.[19] Another disadvantage is related to the proton transport through the membrane. Water enables the proton transport through the membrane, and therefore the membrane always needs to be hydrated.[20] Therefore, the resulting hydrogen gas is saturated with water which can be an issue depending on the application. The International Organization for Standardization (ISO) stated that water provides a transport mechanism for water-soluble contaminants such as K^+ and Na^+ when present as an aerosol.[21] Both K^+ and Na^+ can affect the fuel cell and are not recommended to exceed 0.05 μmol K^+ or Na^+ per mol hydrogen fuel mixture.[21] To avoid potential issues, the ISO has directed the maximum allowed concentration of impurities for gaseous hydrogen, including water in Table 1 of the ISO 14687-2:2012.[21] The maximum concentration of water in the gaseous hydrogen, used for PEM fuel cells in road vehicles is limited to 5 μmol water per mol hydrogen fuel mixture.[21] This poses two important questions. (1) What is the solubility of water in hydrogen at high pressures close to ambient temperatures? (2) If this solubility is too large, what is the best method to reduce the water content? To answer these questions, an accurate description of the vapor liquid equilibrium (VLE) of the H_2O-H_2 system at high pressures is required. Published experimental data that describe these systems is scarce. To the best of our knowledge, the only experimental data describing phase coexistence of H_2O-H_2 for pressures exceeding 300 bar are from 1927 (limited to $T = 323$ K[22]). At this temperature, hydrogen is supercritical. Wiebe and Gaddy studied also the solubility of hydrogen gas in liquid water at high pressures up to $P = 1013.25$ bar.[23] Therefore, molecular simulation and thermodynamic modeling are needed to determine the water content in compressed hydrogen. In industrial applications, cubic type equations of state (EoS) are one the most commonly used methods to study VLE, because of their simplicity.[24−28] In this work, the Peng−Robinson (PR) EoS and the Soave−Redlich−Kwong (SRK) EoS with van der Waals mixing rules are used to predict the phase coexistence of H_2O-H_2 at elevated pressures. However, molar volumes of the liquid phase and fugacity coefficients at high pressures obtained from PR-EoS and SRK-EoS modeling are known to deviate significantly from experimental values.[29−32]

In this work, it is shown that both the PR-EoS and SRK-EoS fail to describe the liquid phase and the gas phase compositions, with or without fitted binary interaction parameters (k_{ij} values). Since water is a highly polar molecule, either modifications of the conventional mixing rules are required,[25] or more physically based models (i.e., SAFT-types EoS[33] or molecular simulations[34]) should be used to describe the phase behavior of the H_2O-H_2 system.[33] It was found that a temperature-dependent parameter k_{ij} is still required for SAFT-type EoS modeling.[35] Therefore, force-field-based molecular simulation could be considered as a natural tool to study the phase coexistence of the H_2O-H_2 system. In this work, different molecular force fields for water and hydrogen are considered for describing the phase coexistence compositions of the liquid and gas phase of the H_2O-H_2 system, especially at high pressures. To evaluate the accuracy of the

results from molecular simulations, we have performed an extensive literature survey on the VLE of H_2O−H_2 mixtures at high pressures.[22,23,36−43] In this work, it is shown that the best predictions of the VLE of the H_2O−H_2 system at high pressures (in both phases) are obtained using molecular simulations. No adjustable k_{ij} values were used for molecular simulations in this study.

This paper is organized as follows. In section 2, the molecular simulation techniques used in this study are explained and simulation details (molecular simulations and EoS modeling) and force field details for water and hydrogen are provided. Our results obtained from molecular simulations and EoS modeling are presented and compared to experimental data in section 3. Our conclusions are summarized in section 4. In the Supporting Information, we present a detailed overview of available experimental VLE and solubility data for the H_2O−H_2 system at high pressures.

2. MODELING AND METHODOLOGY

2.1. Simulation Techniques. A convenient choice for VLE calculations is the Gibbs Ensemble (GE) method introduced by Panagiotopoulos,[44−46] which is used extensively in molecular simulation studies.[34] In the GE, the vapor and liquid phase are simulated in two simulation boxes, which can exchange molecules, volume, and energy. At coexistence, the pressures, temperatures, and chemical potentials of each component are equal in both boxes.[34] The GE is reliable, and the finite size effects are small unless conditions close to the critical point are considered.[47,48] To accurately predict coexistence densities, simulations in the GE rely on sufficient molecule exchanges between the two phases.[34,45] The well-known drawback of the conventional GE is that at high densities, particle insertions/deletions have a low acceptance probability, also leading to poor estimates of chemical potentials in both phases. Although chemical potentials of different component types are not strictly needed for calculating the coexistence densities, the equality of chemical potentials is an important condition for phase equilibrium. Chemical potential calculations in the GE follow from a modification of the Widom's Test Particle Insertion (WTPI),[34,49] taking fluctuations in density into account. It is well-known that the WTPI method often performs poorly for dense liquids.[50,51]

On the basis of the work of Shi and Maginn,[52,53] Vlugt and co-workers expanded the conventional GE with so-called fractional molecules to improve the efficiency of molecule exchanges between the simulation boxes.[54,55] In contrast to the normal or "whole" molecules, the interactions of fractional molecules are scaled between zero and one with a coupling parameter λ_i. $\lambda_i = 0$ means that the fractional molecule of type i has no interactions with the surrounding molecules and acts as an ideal gas molecule. $\lambda_i = 1$ means that the fractional molecule of type i has fully scaled interactions and interacts as a whole molecule. The fractional molecule of each component type can be in either one of the phases.[54] In addition to conventional thermalization trial moves (translation, rotation, and volume changes), three additional trial moves are associated with the fractional molecule of each component: (1) changes in λ_i while keeping the positions and orientations of all molecules including the fractional molecule(s) fixed; (2) reinsertion of the fractional molecule to a randomly selected position in the other simulation box (phase) while keeping the value of λ_i, positions and orientations of all other molecules

fixed; (3) changing the identity of the fractional molecule with a randomly selected molecule of the same type in the other box, while keeping the value of λ_i, positions, and orientations of all molecules fixed. Biasing using a weight function $W(\lambda_i)$ is used to ensure that the observed probability distribution of λ_i is flat.[54] The use of fractional molecules significantly improves molecule exchanges between the simulation boxes, and thereby the efficiency of the VLE calculations and the calculations of chemical potentials at coexistence. When the number of fractional molecules is less than 1% of the number of whole molecules, the continuous fractional component GE (CFCGE) and the conventional GE yield identical coexistence densities.[56] Fractional molecules should not be counted when computing mole fractions.[57] One can show that computed chemical potentials in CFCGE and the conventional GE are identical.[54] For further details and a comparison between the conventional GE and CFCGE, the reader is referred to refs 50, 54, 58, and 59.

Since molecule exchanges in the CFCGE are performed using fractional molecules with scaled interactions, molecule transfers between coexisting phases are facilitated leading to a more efficient sampling of coexistence densities. The chemical potential of component type i in phase j (gas or liquid) is obtained from[54,55]

$$\mu_{ij} = k_B T \ln \frac{\langle \rho_{ij} \rangle}{\rho_0} - k_B T \ln \left(\frac{p(\lambda_{ij} = 1)}{p(\lambda_{ij} = 0)} \right) \tag{1}$$

where k_B is the Boltzmann constant, ρ_{ij} is the number density of component i in phase j and $p(\lambda_{ij})$ is the (unbiased) Boltzmann probability distribution of λ_{ij} in phase j. The term ρ_0 is an arbitrary reference density to make the argument of the logarithm dimensionless. The first term on the right-hand side of eq 1 is the ideal gas contribution of the chemical potential (μ_{ij}^{id}). The second term on the right-hand side of eq 1 is the excess chemical potential (μ_{ij}^{ex}). The brackets $\langle \cdots \rangle$ denote an ensemble average. The fugacity coefficient of component type i in phase j follows from

$$\phi_{ij} = \frac{1}{Z_{mix}} \times \frac{p(\lambda_{ij} = 0)}{p(\lambda_{ij} = 1)} \tag{2}$$

where Z_{mix} is the compressibility factor of the mixture. Equation 2 is derived in the Supporting Information. On the basis of the limited experimental solubility data available in the literature at T = 323 K and pressures above P = 300 bar,[22] we know that the solubility of water in the gas phase at high pressures (P = 100 bar to P = 1000 bar) is about a couple of hundred ppm's (molar) or less. At lower temperatures, due to the low solubility of water in hydrogen, a very large number of hydrogen molecules (up to a million) in the gas phase would be required in the simulations to have on average a single water molecule in the gas phase. The solubility of hydrogen in the liquid phase is also very low, for example, mole fractions ranging from between 0.003 and 0.115 at T = 323 K and pressures between P = 25 bar and P = 1000 bar. This makes most simulations of the H_2O−H_2 system in the CFCGE at low temperatures and high pressures impractical, as a very large system is needed to have at least a single component of each type in each box. One could in principle simulate the VLE of H_2O−H_2 in the CFCGE using a smaller system size. This would lead to poor statistics for the average number of H_2 molecules in the liquid phase, and H_2O molecules in the gas

phase. To circumvent these issues, both the gas and liquid phases (almost pure hydrogen gas and pure liquid water, respectively) are simulated independently in the continuous fractional component NPT (CFCNPT) ensemble.[58] By varying the mixture composition in the gas and liquid phases around the equilibrium state, the coexistence compositions are obtained by imposing equal chemical potentials for both phases. Vlugt and co-workers considered the conventional NPT ensemble expanded with a fractional molecule,[58] similar to earlier work with the GE.[54] Similar to the CFCGE, trial moves for the fractional molecule are performed in addition to the usual thermalization moves. The only difference is that in the simulations in the CFCNPT ensemble, the trial moves related to the fractional molecule are performed in the same simulation box. By applying the CFCMC method to the NPT ensemble, one can calculate the chemical potential of each species (similar to eq 1). For details the reader is referred to refs 58 and 60.

At high pressures we know that the solute is almost pure in both phases, that is, hydrogen in the gas phase and water in the liquid phase. For a solution close to infinite dilution, one can express the variation of the excess chemical potential of the solute, that is, hydrogen in the liquid phase and water in the gas phase as a function of the number density of the solute:

$$\mu_{ij}^{\mathrm{ex}}(\rho_{ij}) = A_{ij} + B_{ij}\rho_{ij} + C_{ij}\rho_{ij}^2 + \cdots \tag{3}$$

To obtain the terms A_{ij}, B_{ij}, $\cdots$, multiple simulations are performed at constant temperature and pressure, for different concentrations of the solute. In the region of interest (very dilute solutions) $\mu_{ij}^{\mathrm{ex}}(\rho_{ij})$ depends linearly on the number density. As the solvent in both phases is almost a pure component, one can assume that the excess chemical potential of the solvent is independent of the number of few solute molecules in that phase. The coexistence densities are then obtained by imposing equal chemical potentials of each component using eq 3. Note that at conditions at which both methods are applicable to obtain phase coexistence (i.e., simulations in the GE and the CFCNPT ensemble), we have verified that both methods (i.e., GE and imposing equal chemical potentials) yield the same results. Obtaining chemical potentials from single-box simulations may become less efficient close the critical point.

2.2. Simulation Details. Depending on the temperature and pressure, molecular simulations are performed in the CFCGE or in the CFCNPT ensemble. All simulations were performed using our in-house code. It was verified that our results are identical to those from the RASPA software package.[61,62] In all simulations, periodic boundary conditions were used. All molecules are rigid, and the interactions between the molecules only consist of LJ and Coulombic interactions. LJ potentials were truncated but not shifted. Analytic tail corrections and the Lorentz–Berthelot mixing rules were applied.[34,63] To treat the electrostatic interactions, the Ewald summation was used with a relative precision of 1×10^{-6}. In CFCGE simulations of $H_2O–H_2$ mixtures, fractional molecules of water and hydrogen are present which are used to facilitate molecule exchanges between the phases. To protect the charges from overlapping, the (repulsive) LJ interactions of the fractional molecules are switched on before the electrostatics.[64–69] For details about scaling the LJ and Coulombic interactions of the fractional molecule, the reader is referred to refs 55, 56, and 60. Details about the force field parameters for

different water and hydrogen models and cutoff radii for LJ interactions are provided in Tables S1 and S2 of the Supporting Information. For simulating hydrogen at low temperatures, it is important to consider quantum effects, for example, by using a (temperature-dependent) Feynman-Hibbs effective interaction potential.[70–72] However, at the temperatures considered here quantum effects are small and can be safely neglected.

Simulations in the CFCGE were started with 730 molecules of water and 600 molecules of hydrogen. For all temperatures and pressures, 10^5 equilibration cycles were carried out followed by 4×10^6 production cycles. Each MC cycle consists of N_{MC} Monte Carlo trial moves, where N_{MC} equals the total number of molecules, with a minimum of 20. Trial moves in the CFCGE simulations were selected with the following probabilities: 1% volume changes, 35% translations, 30% rotations, 17% λ changes, 8.5% reinsertions of fractional molecules at randomly selected positions in the other box, and 8.5% identity changes of fractional molecules between the boxes. Independent CFCNPT simulations of the liquid phase, close to infinite dilution of hydrogen, were performed with 730 water molecules with $N_{\mathrm{H_2}} \in \langle 0,10 \rangle$ hydrogen molecules. Similarly, independent CFCNPT simulations of the gas phase, close to infinite dilution of water, were performed with 600 hydrogen molecules with $N_{\mathrm{H_2O}} \in \langle 0,7 \rangle$ water molecules. Trial moves in the CFCNPT simulations were selected with the following probabilities: 1% volume changes, 35% translations, 30% rotations, 17% λ changes, 8.5% reinsertions of fractional molecules at randomly selected positions, and 8.5% identity changes of fractional molecules. Uncertainties of ensemble averages were computed by performing five independent simulations and recording standard deviations.

2.3. Force Fields. To model the VLE of $H_2O–H_2$ mixtures, molecular force fields are considered to predict the density and composition of the gas and liquid phases. As the most commonly used force fields are developed based on single-phase coexistence data,[73,74] we have screened these force fields using single-phase hydrogen (gas phase) and single-phase water (liquid phase) simulations. Force fields for water and hydrogen are selected based on predicting bulk properties of pure phases such as densities, chemical potentials, and fugacity coefficients. The densities and fugacity coefficients of molecular hydrogen in the gas phase are computed at different pressures using several force fields from the literature. The results are compared with REFPROP.[75,76] Common force fields for molecular hydrogen in the literature include single site,[77–79] two-site,[80] and multisite potentials with (permanent) charge interactions.[81–83] Single-site hydrogen models are capable of predicting bulk thermodynamic properties of hydrogen accurately. The single-site hydrogen model by Buch[77] reproduces the bulk properties of hydrogen accurately up to high pressures. Multisite hydrogen potentials that consider charge-quadrupoles and polarizability are more relevant for modeling hydrogen sorption in highly heterogeneous systems.[80,81,83–86] The densities and the excess chemical potentials predicted by different force fields of water in the liquid phase are computed as a function of pressure. The results are compared to those obtained from REFPROP.[75,87] Even though water is a flexible and polarizable molecule, to date most molecular simulation studies consider rigid molecular potentials of water with constant point-charges.[74,88–91] It is computationally advantageous to use

these simplified water potentials, which can predict thermodynamic and transport properties of water in good agreement with experiments. To obtain a more physical description of water, polarizable force fields have been developed to account for polarization effects.[74,92−101] Compared to the fixed-charge water potentials, thermodynamic properties of polarizable force fields are not fully known.[93] Commonly used fixed-charge force fields for water are three-site potentials TIP3P,[102] SPC,[103,104] and SPC/E;[105] four-site potentials TIP4P/2005,[89] TIP4P/Ew,[106] and OPC;[73] and a five-site potential TIP5P/Ew.[107] In our previous studies,[50,60] we have shown that the computed excess chemical potentials of water for the three-site potentials TIP3P and SPC are in good agreement with values obtained from an empirical Helmholtz equation of state[87] based on experimental data.[76] It is well-known that the TIP4P/2005 water outperforms the three-site models for predicting bulk properties of water such as the density.[89] In our previous studies, we have shown that the computed excess chemical potentials of water obtained from four-site and five-site potentials show larger deviations from experimental data compared to three-site potentials.[50]

2.4. Equation of State Modeling. The PR-EoS[108] and SRK-EoS[109] with the conventional van der Waals mixing rules are used to predict the VLE of H_2O−H_2 mixtures. These equations of state are the most widely used in industry and perform best for describing the VLE of nonpolar mixtures.[110] It is well-known that the molar volume of the liquid phase predicted by the cubic equations of state is inaccurate.[111,112] Since the solubility of small nonpolar gas molecules in the liquid phase are dominated by entropic effects (i.e., molar volume), the solubility of H_2 in H_2O is predicted poorly. We have used both zero k_{ij} values and k_{ij} values fitted on high pressure experimental data. Details on the EoS modeling are provided in the Supporting Information.

3. RESULTS AND DISCUSSION

3.1. Molecular Simulations. The densities and fugacity coefficients of pure hydrogen between $P = 100$ bar and $P = 1000$ bar obtained from CFCNPT simulations and EoS modeling are compared to those obtained from REFPROP,[113] see Figure 1. Since the differences between the results obtained for $P < 400$ bar are very small, only the results between $P = 400$ bar and $P = 1000$ bar are shown. The raw data are provided in Table S3. Hydrogen models used for this study include single-site models such as Hirschfelder,[78] Vrabec,[79] Buch,[77] two-site model such as Cracknell,[80] and the multisite model of Marx.[83] It is clear that the densities obtained using the Buch[77] and Marx[83] force fields are in excellent agreement with experimental data up to $P = 1000$ bar. The results obtained from the PR-EoS and SRK-EoS deviate from experimental data for $P > 400$ bar. The calculated fugacity coefficients of pure hydrogen in the gas phase are best predicted using the Buch[77] and Marx[83] force fields. The calculated fugacity coefficients from the SRK-EoS are in excellent agreement with experiments. The simulation results show that both the Buch and Marx force fields outperform the other molecular models in predicting bulk densities and fugacity coefficients of hydrogen at high pressures. This means that considering a quadrupole moment for hydrogen does not strictly improve the bulk properties of hydrogen in the gas phase. Including the quadrupole moment may improve the prediction of phase coexistence in the liquid phase, as observed by Sun et al.[35]
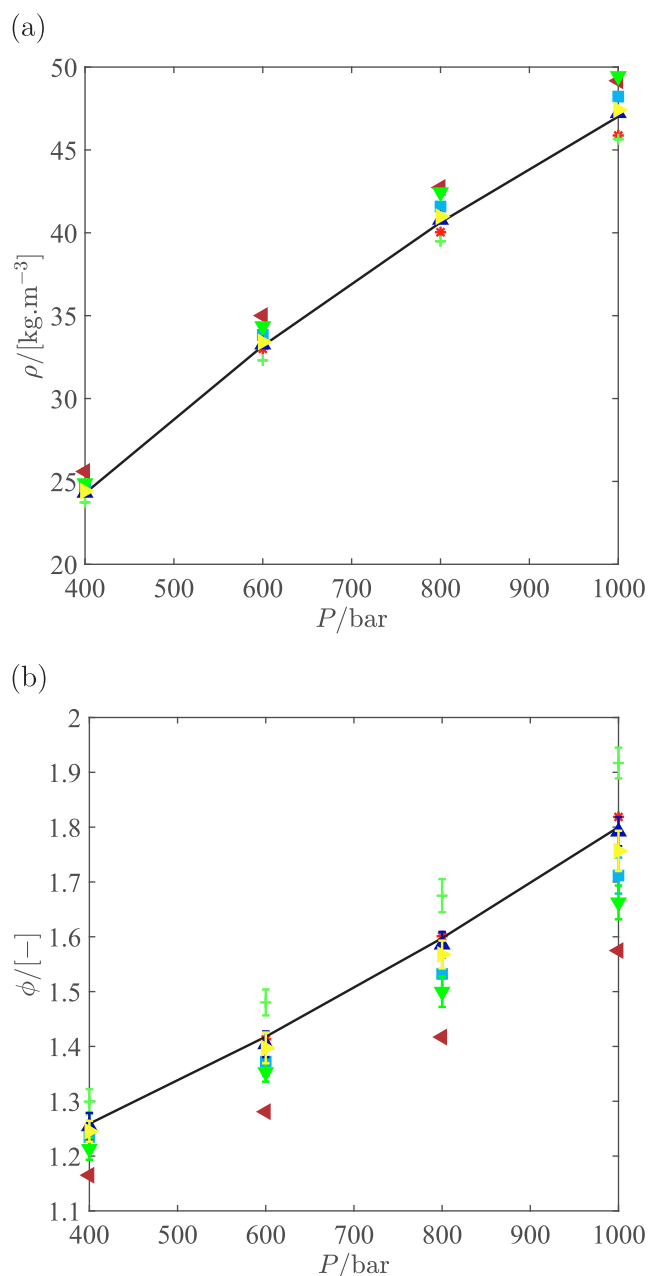

Figure 1. Comparison of different models to predict (a) the density and (b) the fugacity coefficient of pure hydrogen in the gas phase at $T = 323$ K and pressures ranging between $P = 10$ and $P = 1000$ bar. PR-EoS (left-pointing triangle), SRK-EoS (asterisk), experimental data from REFPROP[75,76] (lines). Molecular force fields: Hirschfelder[78] (squares), Vrabec[79] (Plus signs), Buch[77] (upward-pointing triangles), Cracknell[80] (downward-pointing triangles), and Marx[83] (right-pointing triangles). Parameters for the EoS are provided in Table S10. Raw simulation data are provided in Table S3.

Therefore, the Marx force field is considered further for VLE simulations of H_2O−H_2 mixtures.

The densities and chemical potentials of TIP3P,[102] SPC,[104] SPC/E,[105] TIP4P/2005,[89] TIP4P/Ew,[114] OPC,[73] and TIP5P/Ew[107] force fields between $P = 100$ bar and $P = 1000$ bar obtained from CFCNPT simulations are compared to the IAPWS empirical EoS,[75,87] see Figure 2. Raw data are provided in Table S4. It is shown in Figure 2a that the force fields TIP5P/Ew and TIP4P/2005 clearly outperform the TIP3P and SPC force fields in predicting the density of liquid water
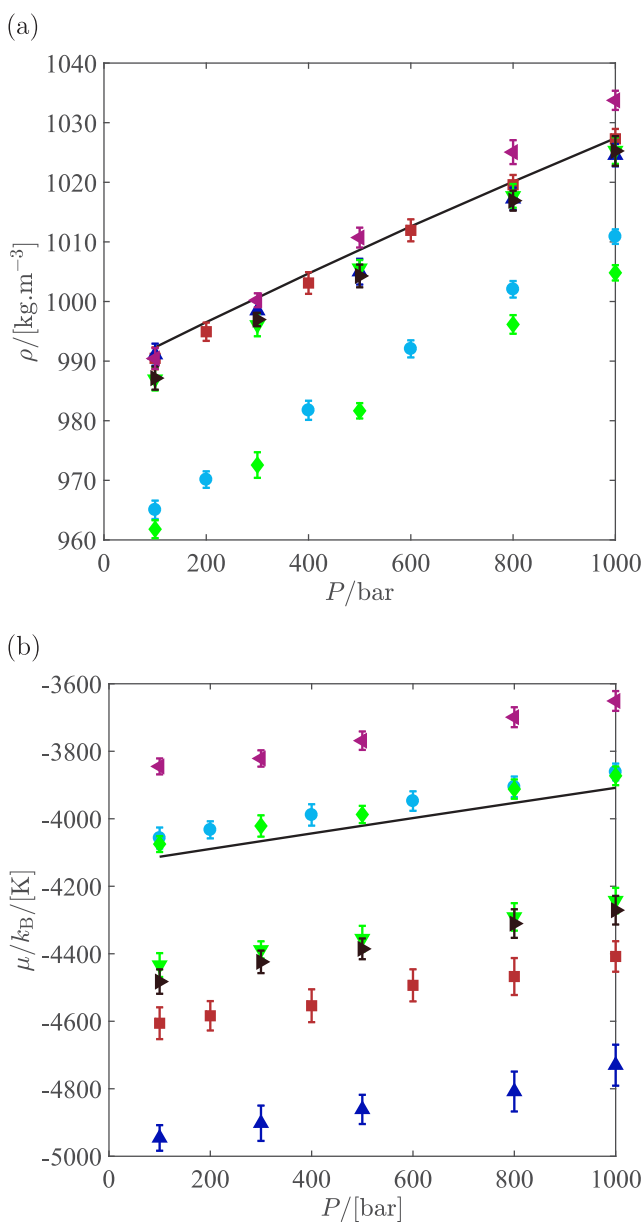
(a)

(b)

Figure 2. Comparison of different force fields of water to predict (a) the density and (b) the chemical potential in the liquid phase at $T = 323$ K and pressures ranging between $P = 10$ and $P = 1000$ bar: TIP3P[102] (diamonds), SPC[104] (circles), SPC/E[105] (right-pointing triangles), TIP4P/2005[89] (squares), TIP4P/Ew[114] (downward-pointing triangles), OPC[73] (upward-pointing triangles), TIP5P/Ew[107] (left-pointing triangles). In both subfigures, the lines are obtained from REFPROP.[75,76] Raw data are provided in Table S4.

(on average ca. 2%) over the whole pressure range. The TIP4P/2005 water model is parametrized based on temperature of maximum density of liquid water, the stability of several ice polymorphs, etc.[89] The TIP5P/Ew model is obtained from reparametrization of the TIP5P model[115] which is also a very accurate model capable of predicting maximum density of liquid water at ca. 4 °C.[107] Note that the deviations of the densities obtained from the TIP3P and SPC models decrease with increasing pressure. As shown in Figure 2, the chemical potential of water is best predicted using the TIP3P and SPC force fields over the whole temperature range. This observation is also in agreement with previous works.[50,60]

The performances of the TIP3P and the SPC force fields are very similar in calculating the densities and chemical potentials of water. The TIP3P force field has been parametrized to the vaporization energy and density of liquid water.[102] This is consistent with the fact that the computed chemical potential of TIP3P water is in better agreement with IAPWS empirical EoS, compared to the TIP4P/2005 or TIP5P/Ew models. Raw data for Figure 2 are provided in Table S4. As shown in Figure 2, the average deviation of the chemical potential of the TIP3P force field from the IAPWS empirical EoS[75,87] is about +50 K (in units of energy/k_B) for the whole pressure range. The average deviations of the chemical potentials for the TIP4P/2005 and TIP5P/Ew force fields from IAPWS empirical EoS are ca. −500 K and +250 K (in units of energy/k_B), respectively. The performance of the SPC/E force field is very similar to that of the TIP4P/2005 force field for predicting the densities and chemical potentials of water. For the 4-site water force fields, the densities and chemical potentials of the TIP4P/2005 force field show the best agreement with the experiments. Due to the overall difference between the predicted densities and chemical potentials of these water models, it is not a priori clear which water model is best fitted for predicting the VLE of H_2O-H_2 mixtures. Therefore, three water models are considered (TIP3P, TIP4P/2005, TIP5P/Ew) in combination with the Marx force field (for hydrogen) for phase coexistence calculations of H_2O-H_2 mixtures, using molecular simulations.

The water content in the gas phase and the solubility of hydrogen in the liquid phase for the mixture defined by the TIP3P-Marx force fields are obtained from phase coexistence equilibrium calculations, see Figure 3. The corresponding $P-x-y$ diagram is shown in Figure S1. To check the consistency between the results with both methods, phase coexistence calculations at $T = 323$ K and $P > 100$ bar are performed for both (i.e., CFCGE and CFCNPT). It is shown that both methods yield the same results within the error bars. At $T = 283$ K, all simulations are performed only in the CFCNPT ensemble for the whole pressure range. At $T = 310$ K and $P > 100$ bar, phase coexistence calculations are also performed using simulations in the CFCNPT ensemble. At $T = 366$ K and $T = 423$ K, phase coexistence calculations are performed using simulations in the CFCGE. Raw data from experimental results are provided in Tables S5 and S6, and the simulations results are provided in Table S7. On the basis of the available experimental data at pressures above $P = 300$ bar,[22] it is clear that the predicted solubility of TIP3P water in the gas phase is in good agreement with experimental data. At $T = 283$ K, no experimental solubilities have been found, and therefore only the results obtained from molecular simulations are shown. For all isotherms of water vapor in the gas phase, it can be observed that the water content is slightly overpredicted at low pressures. At high pressures, the solubility of water in the gas phase is marginally underpredicted. From the condition of chemical equilibrium, we know that the chemical potential of water in the gas phase is equal to the chemical potential of water in the liquid phase. Therefore, it seems that good performance of the TIP3P force field to predict the isotherms of water in the gas phase is most likely related to how accurate it can predict μ_{H_2O} in the liquid phase. On the basis of the results shown in Figures 2 and 3 it can be concluded that parametrization of the TIP3P force field based on the evaporation energy as one of the target quantities is essential
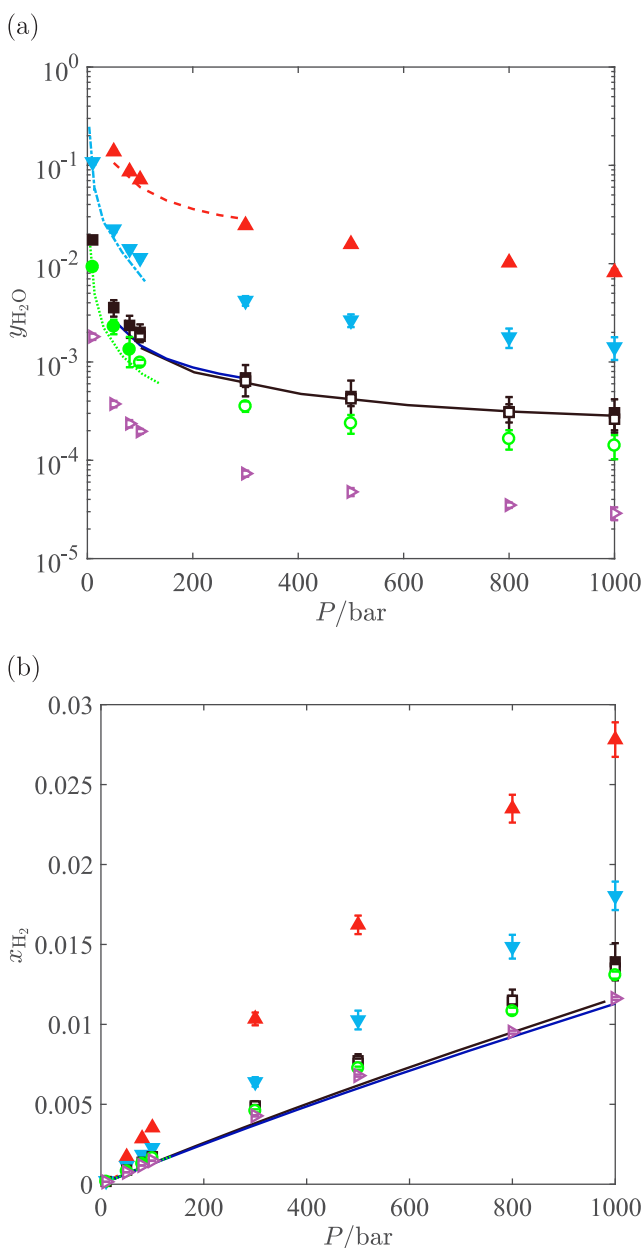
(a)

(b)

Figure 3. Vapor−liquid equilibrium of H_2O−H_2 (TIP3P[102]-Marx[83]) at pressures ranging between P = 10 and P = 1000 bar. (a) y_{H_2O} in the gas phase and (b) x_{H_2} in the liquid phase. T = 423 K (upward-pointing triangles), T = 366 K (downward-pointing triangles), T = 323 K (squares), T = 310 K (circles), T = 283 (right-pointing triangles). Experimental data[22,23,37−41,43] for T = [423, 366, 323, 310] K are shown with dashed lines, dash-dot lines, solid lines, and dotted lines, respectively. Published high pressure data are only available for T = 323 K.[22] Raw data are provided in Tables S5, S6, and S7.

for predicting the VLE of H_2O−H_2 mixtures. For all temperatures in this study (between T = 283 K and T = 423 K), it is observed that the solubility of water in the gas phase at coexistence is significantly higher than 5 μmol water per mol hydrogen (as allowed by the ISO 14687-2:2012 standard[21]). Therefore, an additional step for removing water is needed.

The calculated isotherms for hydrogen in the liquid phase (TIP3P-Marx) are clearly overpredicted compared to experimental data as shown in Figure 3b. To the best of our knowledge, experimental solubility data for hydrogen iso-

therms in the liquid phase at pressures above ca. P = 140 bar are not available in the literature, except at T = 323 K.[22] The deviation from experimental solubilities of hydrogen at T = 323 K ranges from about 36% to 18% between P = 50 bar and P = 1000 bar, respectively. At T = 366 K, the deviation from experimental data is about 50% between P = 50 bar and P = 100 bar. At T = 423 K the deviation from experimental data is about 110% between P = 50 bar and P = 80 bar. Therefore, it can be concluded that the deviation of simulation results from experimental data increases with increasing temperature. On the basis of these results, it can also be concluded that the deviation from experimental solubilities decreases with increasing pressure. Similarly, better agreement is observed between experimental densities of water and those obtained based on TIP3P water at high pressures, as also shown in Figure 2. This suggests that predicting the density of the liquid phase (almost pure water) accurately may result in predicting the mixture compositions in better agreement with experiments.

The solubilities obtained from phase coexistence at equilibrium for the H_2O−H_2 mixture defined by the TIP4P/2005-Marx force fields are shown in Figure 4. Raw data are provided in Table S8. For this mixture, all simulations are performed in the CFCGE, at T = 323 K, T = 366 K, and T = 423 K. It is clear from Figure 4 that the solubilities of water in the gas phase are significantly underestimated for the whole pressure range. This is mainly due to the fact that the chemical potential of TIP4P/2005 water is significantly underpredicted, as shown in Figure 2. Since the predicted water solubilities in the gas phase are systematically lower for the TIP4P/2005-Marx mixture (see Figures 3a and 4a), the statistics for water solubilities obtained from CFCGE simulations are worse. This sampling issue is explained in section 2.1. Similarly, the computed isotherms of hydrogen in the liquid phase are slightly underpredicted. For the mixture defined by TIP4P2005-Marx force fields, better agreement with experiments is observed for solubilities in the liquid phase for all temperatures. At T = 366 K, the deviation from experimental data is about 14% between P = 50 bar and P = 100 bar. At T = 423 K the deviation from experimental data is about 5% between P = 50 bar and P = 80 bar.

The solubilities obtained from phase coexistence at equilibrium for H_2O−H_2 mixture defined by TIP5P/Ew-Marx force fields are shown in Figure 5. Raw data are provided in Table S9. For this system, all simulations are performed in the CFCGE, at T = 323 K, T = 366 K, and T = 423 K. In sharp contrast to the TIP4P/2005-Marx system, both calculated solubilities in the liquid and gas using the TIP5P/Ew-Marx system are overpredicted. The solubilities of hydrogen in the liquid phase are very similar to those obtained form the TIP3P-Marx force fields. To explain the results in a coherent way, it is important to consider the predicted water isotherms in the gas phase in Figures 3 to 5 and the calculated chemical potentials of pure water in Figure 2b simultaneously. From these figures, it can be concluded that underpredicting the solubilties in the gas phase is directly related to underpredicting the chemical potential of water (TIP4P/2005). Similarly, overpredicting the solubilties of water in the gas phase is directly related to overpredicting the chemical potential of water (TIP5P/Ew).

3.2. Equation of State Modeling. The water content in the gas phase and the solubility of hydrogen in the liquid phase are also calculated using the PR-EoS and SRK-EoS. High pressure experimental solubilites at T = 323 K were used to
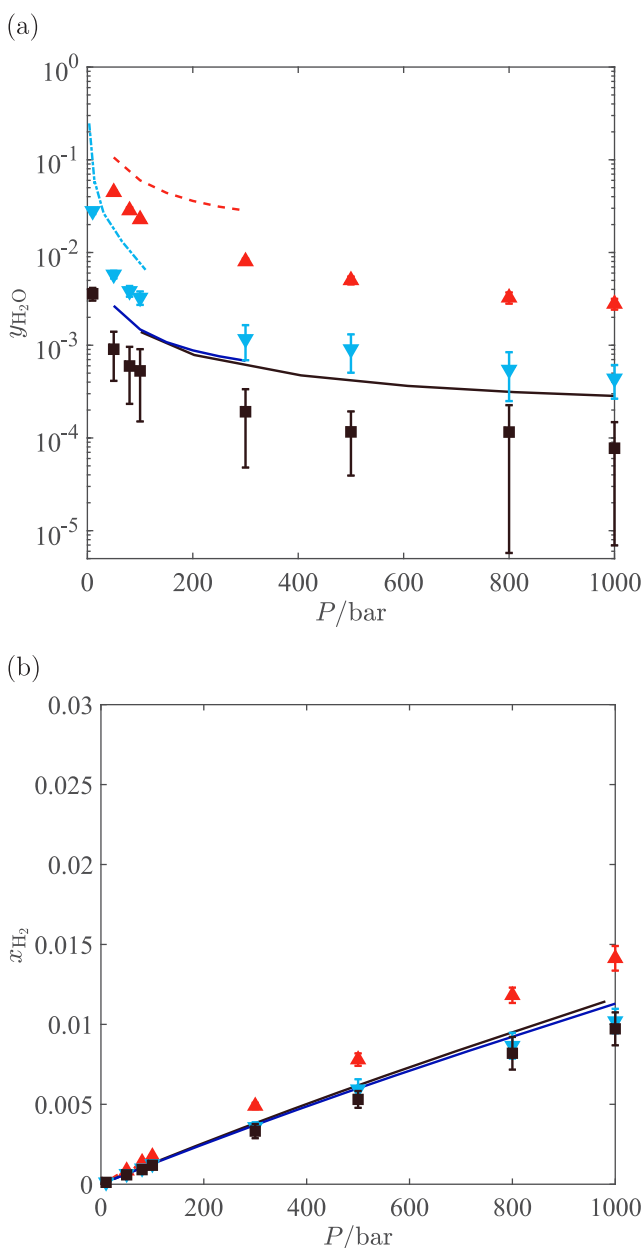
Figure 4. Vapor−Liquid equilibrium of H_2O−H_2 (TIP4P/2005[89]-Marx[83]) at pressures ranging between P = 10 and P = 1000 bar. (a) y_{H_2O} in the gas phase and (b) x_{H_2} in the liquid phase. T = 423 K (upward-pointing triangles), T = 366 K (downward-pointing triangles), T = 323 K (squares). Experimental data[22,23,37−41,43] for T = [423, 366, 323, 310] K are shown with dashed lines, dash-dot lines, solid lines, and dotted lines (if available), respectively. Published high pressure data are only available for T = 323 K.[22] Raw data are provided in Tables S5, S6, and S8.

Figure 5. Vapor−liquid equilibrium of H_2O−H_2 (TIP5P/Ew[107]-Marx[83]) at pressures ranging between P = 10 and P = 1000 bar. (a) y_{H_2O} in the gas phase and (b) x_{H_2} in the liquid phase. T = 423 K (upward-pointing triangles), T = 366 K (downward-pointing triangles), T = 323 K (squares). Experimental data[22,23,37−41,43] for T = [423, 366, 323, 310] K are shown with dashed lines, dash-dot lines, solid lines, and dotted lines (if available), respectively. Published high pressure data are only available for T = 323 K.[22] Raw data are provided in Tables S5, S6, and S9.

obtain the binary interaction parameters (k_{ij} values) for the PR-EoS and SRK-EoS. For T = 323 K, the isotherms of water and hydrogen in the gas and liquid phase are shown in Figure 6 using both zero k_{ij} values and nonzero k_{ij} values. In Figure 6, it is shown that the predicted solubilities in the liquid phase are significantly lower compared to experiments, using zero k_{ij} values. The solubility of (nonpolar) gases is dominated by entropic effects which are related to the molar volume.[116] Although cubic equations of state are popular in industry,[24] it is well-known that the predicted volumes of the liquid phase
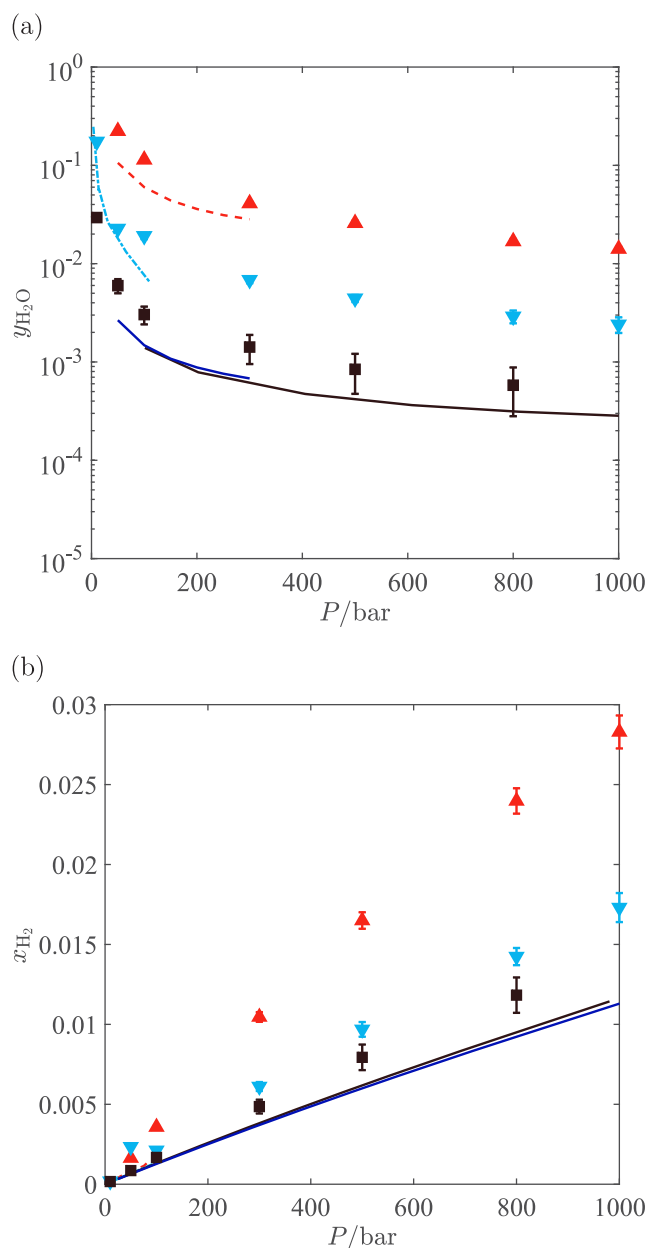
from PR-EoS or SRK-EoS have significant differences with experimental data.[25,26,112] Up until now, more than 220 modifications of mixing rules for pure components and extensions to mixtures with the PR-EoS have been reported in literature.[25] This clearly indicates the need for more physically based models for thermodynamic modeling. In addition, the H_2O−H_2 system is highly polar in the liquid phase, and the performance of the conventional mixing rules for PR-EoS and SRK-EoS for polar mixture are known to be poor.[25] Therefore, it is expected that PR-EoS or SRK-EoS are
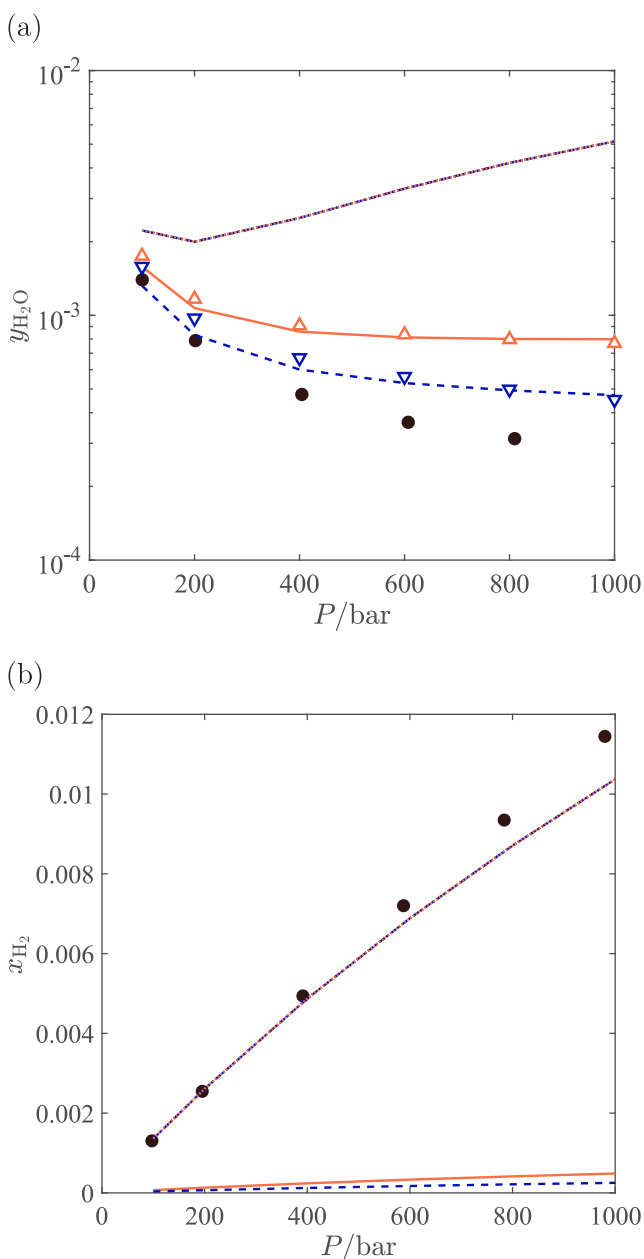
(a)

(b)

Figure 6. VLE of H_2O-H_2 at $T = 323$ K and pressures ranging between $P = 100$ and $P = 1000$ bar, obtained from EoS modeling. (a) mole fraction of water in the gas phase, (b) mole fraction of hydrogen in the liquid phase. Experimental solubilities[22,23] are shown with circles. In both subfigures, the results are shown for $k_{ij} = 0$: PR-EoS[108] (lines), SRK-EoS[109] (dashed lines). The results from the $\gamma-\phi$ method are shown with open symbols: PR-EoS (upward-pointing triangles) and the SRK-EoS (downward-pointing triangles). The results for the fitted BIP for the PR-EoS ($k_{ij} = -0.89$) are shown with dash-dot lines. The results for the fitted BIP for the SRK-EoS ($k_{ij} = -1.51$) are shown with dotted lines.

not able to predict solubilities of hydrogen in liquid water accurately. With the fitted k_{ij} values, the obtained solubilities of hydrogen in the liquid phase are in excellent agreement with experimental data for $p < 400$ bar. However, the solubilities in the gas phase deviate significantly using the fitted k_{ij} values. Therefore, calculations of VLE of H_2O-H_2 mixtures using PR-EoS and SRK-EoS do not yield satisfactory results for both phases simultaneously, with or without adjusted k_{ij} values.

4. CONCLUSIONS

Molecular simulations are used to model the VLE behavior of H_2O-H_2 mixtures for pressures between $P = 10$ bar and $P = 1000$ bar. In Tables S5 and S6, a detailed overview of available experimental data has been provided for this system. It is shown that commonly used cubic equations of state, with conventional mixing rules fail to predict the composition of the gas and the liquid phases accurately. For the different molecular models for hydrogen, the Buch force field[77] (single-site model) and the Marx force field (including quadrupole moment) predict the density and fugacity coefficient of hydrogen in good agreement with experiments up to $P = 1000$ bar. In this study, no force field for rigid water with fixed point charges could accurately predict both the chemical potential and the density of water. The computed chemical potentials of TIP3P water[102] have the best agreement with experimental data from REFPROP[75] with a deviation of ca. +50 K (in units of energy/k_B) for pressures between $P = 100$ bar and $P = 1000$ bar. This may be partly due to the fact that one of the target fitting parameters for the TIP3P force field is the heat of vaporization, unlike the TIP4P/2005 and TIP5P/Ew force fields. The computed chemical potentials (in units of energy/k_B) of the TIP4P/2005 and TIP5P/Ew deviate on average by −500 K and +250 K from experimental data in this pressure range, respectively. Both the TIP4P/2005 and TIP5P/Ew force fields can predict the density of liquid water in good agreement with the experiments for the whole pressure range. From the simulation results, it is observed that solubilities of water in the gas phase are systematically underpredicted when using the TIP4P/2005 force field. This force field also underpredicts the chemical potential of liquid water compared to experiments. The highest solubilities in the gas phase are predicted using the TIP5P/Ew force field with the largest values for the calculated chemical potential of water. The best agreement between the predicted gas phase compositions and experiments for the whole pressure range is observed for the TIP3P force field. This suggests that a suitable water force field for studying the VLE of H_2O-H_2 mixtures can be screened based on the chemical potential of the water model in the liquid phase. On the basis of the screening of seven water force fields in this study, it turns out that the TIP3P and SPC force fields (with very similar values for chemical potential of liquid water) can best predict the equilibrium vapor phase coexistence composition of the H_2O-H_2 system. For all temperatures in this study, we observed that the solubility of water in the gas phase at coexistence is significantly higher than 5 μmol water per mol hydrogen (as allowed by the ISO standard). Therefore, an additional step for removing water from the gas phase is required. Despite the fact that the molecular simulations significantly outperform cubic EoS modeling for the VLE of H_2O-H_2 mixtures, the predicted liquid phase compositions need further improvements. The solubilities of hydrogen in the liquid phase are overpredicted using the TIP3P-Marx and TIP5P/Ew-Marx force fields. The best agreement between the calculated liquid phase composition and experiments is observed for the TIP4P/2005-Marx system (although the predicted solubilities are slightly lower). Further improvements in simulations of H_2O-H_2 systems may be realized taking polarizability of water molecules into account. Therefore, further molecular simulations of the H_2O-H_2 system are recommended using polarizable force

fields for water, especially to improve the predictions for the liquid phase composition.

■ ASSOCIATED CONTENT

Ⓢ Supporting Information

. The Supporting Information is available free of charge on the ACS Publications website at DOI: 10.1021/acs.jced.9b00513.

> Derivation of eq 2; force field parameters for water and hydrogen; calculated densities and fugacity coefficients for pure hydrogen in the gas phase (different force fields); calculated densities and chemical potentials for pure liquid water (different force fields); experimental solubilities of hydrogen and water vapor in the H_2O-H_2 mixture (liquid phase, gas phase, repectively) at coexistence; compositions of H_2O-H_2 mixtures at equilibrium using MC simulations; equation of state parameters for the PR-EoS and SRK-EoS (PDF)

■ AUTHOR INFORMATION

Corresponding Author
*E-mail: t.j.h.vlugt@tudelft.nl.

ORCID ⬤
Ahmadreza Rahbari: 0000-0002-6474-3028
Mahinder Ramdin: 0000-0002-8476-7035
Othonas A. Moultos: 0000-0001-7477-9684
Thijs J. H. Vlugt: 0000-0003-3059-8712

Notes
The authors declare no competing financial interest.

■ REFERENCES

(1) *World Population Prospects: The 2017 Revision, Key Findings and Advance Tables*, ESA/P/WP/248. 2017; https://population.un.org/wpp/Publications/Files/WPP2017_KeyFindings.pdf (accessed 17/7/2019).

(2) United Nations. Transforming our world: the 2030 Agenda for Sustainable Development. (2015) General Assembly Resolution, A/RES/70/1; http://www.un.org/ga/search/view_doc.asp?symbol=A/RES/70/1&Lang=E (accessed 17/7/2019).

(3) *World Energy Outlook 2018*. 2018; www.iea.org/weo (accessed 17/7/2019).

(4) Adoption of the Paris Agreement, FCCC/CP/2015/L.9/Rev.1. 2015; https://unfccc.int/resource/docs/2015/cop21/eng/l09r01.pdf (accessed 17/7/2019).

(5) Gallo, A.; Simões-Moreira, J.; Costa, H.; Santos, M.; Moutinho dos Santos, E. Energy storage in the energy transition context: A technology review. *Renewable Sustainable Energy Rev.* **2016**, *65*, 800−822.

(6) Zakeri, B.; Syri, S. Electrical energy storage systems: A comparative life cycle cost analysis. *Renewable Sustainable Energy Rev.* **2015**, *42*, 569−596.

(7) Evans, A.; Strezov, V.; Evans, T. J. Assessment of utility energy storage options for increased renewable energy penetration. *Renewable Sustainable Energy Rev.* **2012**, *16*, 4141−4147.

(8) Mahlia, T.; Saktisahdan, T.; Jannifar, A.; Hasan, M.; Matseelar, H. A review of available methods and development on energy storage;

technology update. *Renewable Sustainable Energy Rev.* **2014**, *33*, 532−545.

(9) Chen, H.; Cong, T. N.; Yang, W.; Tan, C.; Li, Y.; Ding, Y. Progress in electrical energy storage system: A critical review. *Prog. Nat. Sci.* **2009**, *19*, 291−312.

(10) Johnston, B.; Mayo, M. C.; Khare, A. Hydrogen: the energy source for the 21st century. *Technovation* **2005**, *25*, 569−585.

(11) Rahbari, A.; Ramdin, M.; van den Broeke, L. J. P.; Vlugt, T. J. H. Combined steam reforming of methane and formic acid To produce syngas with an adjustable H_2:CO ratio. *Ind. Eng. Chem. Res.* **2018**, *57*, 10663−10674.

(12) Adolf, J.; Balzer, C.; Louis, J. *Energy of the Future? Sustainable Mobility through Fuel Cells and H_2*; Shell Deutschland Oil GmbH, 2017.

(13) Bouwman, P. Electrochemical Hydrogen Compression (EHC) solutions for hydrogen infrastructure. *Fuel Cells Bulletin* **2014**, *2014*, 12−16.

(14) HyET Hydrogen BV; https://hyet.nl/hydrogen (accessed 17/7/2019).

(15) Bampaou, M.; Panopoulos, K. D.; Papadopoulos, A. I.; Seferlis, P.; Voutetakis, S. An electrochemical hydrogen compression model. *Chem. Eng. Trans.* **2018**, *70*, 1213.

(16) Ströbel, R.; Oszcipok, M.; Fasil, M.; Rohland, B.; Jörissen, L.; Garche, J. The compression of hydrogen in an electrochemical cell based on a PE fuel cell design. *J. Power Sources* **2002**, *105*, 208−215 7th Ulmer Elektrochemische Tage. .

(17) Suermann, M.; Kiupel, T.; Schmidt, T. J.; Büchi, F. N. Electrochemical hydrogen compression: efficient pressurization concept derived from an energetic evaluation. *J. Electrochem. Soc.* **2017**, *164*, F1187−F1195.

(18) Rohland, B.; Eberle, K.; Ströbel, R.; Scholta, J.; Garche, J. Electrochemical hydrogen compressor. *Electrochim. Acta* **1998**, *43*, 3841−3846.

(19) Nordio, M.; Rizzi, F.; Manzolini, G.; Mulder, M.; Raymakers, L.; Van Sint Annaland, M.; Gallucci, F. Experimental and modelling study of an electrochemical hydrogen compressor. *Chem. Eng. J.* **2019**, *369*, 432−442.

(20) Casati, C.; Longhi, P.; Zanderighi, L.; Bianchi, F. Some fundamental aspects in electrochemical hydrogen purification/compression. *J. Power Sources* **2008**, *180*, 103−113.

(21) *Hydrogen fuel, Product specification, Part 2: Proton exchange membrane (PEM) fuel cell applications for road vehicles*. International Standard, 2012; Vol. *2012*; www.iso.org/committee/54560/x/catalogue/ (accessed 17/7/2019).

(22) Bartlett, E. P. The concentration of water vapor in compressed hydrogen, Nitrogen and a mixture of these gases in the presence of condensed water. *J. Am. Chem. Soc.* **1927**, *49*, 65−78.

(23) Wiebe, R.; Gaddy, V. L. The solubility of hydrogen in water at 0, 50, 75 and 100° from 25 to 1000 atm. *J. Am. Chem. Soc.* **1934**, *56*, 76−79.

(24) Hendriks, E.; Kontogeorgis, G. M.; Dohrn, R.; de Hemptinne, J.-C.; Economou, I. G.; Žilnik, L. F.; Vesovic, V. Industrial requirements for thermodynamics and transport properties. *Ind. Eng. Chem. Res.* **2010**, *49*, 11131−11141.

(25) Lopez-Echeverry, J. S.; Reif-Acherman, S.; Araujo-Lopez, E. Peng-Robinson equation of state: 40 years through cubics. *Fluid Phase Equilib.* **2017**, *447*, 39−71.

(26) Iwai, Y.; Margerum, M. R.; Lu, B. C. Y. A new three-parameter cubic equation of state for polar fluids and fluid mixtures. *Fluid Phase Equilib.* **1988**, *42*, 21−41.

(27) Diamantonis, N. I.; Boulougouris, G. C.; Mansoor, E.; Tsangaris, D. M.; Economou, I. G. Evaluation of cubic, SAFT, and PC-SAFT equations of state for the vapor-liquid equilibrium modeling of CO_2 mixtures with other gases. *Ind. Eng. Chem. Res.* **2013**, *52*, 3933−3942.

(28) Kwak, T.; Mansoori, G. A. Van der Waals mixing rules for cubic equations of state. Applications for supercritical fluid extraction modelling. *Chem. Eng. Sci.* **1986**, *41*, 1303−1309.

(29) Harstad, K. G.; Miller, R. S.; Bellan, J. Efficient high-pressure state equations. *AIChE J.* **1997**, *43*, 1605−1610.

(30) Jhaveri, B. S.; Youngren, G. K. Three-parameter modification of the Peng-Robinson equation of state to improve volumetric predictions. *SPE Reservoir Eng.* **1988**, *3*, 1033−1040.

(31) Poling, B. E.; Prausnitz, J. M.; O'Connell, J. P. *The properties of gases and liquids*, 5th ed.; McGraw-Hill New York: New York, USA, 2001.

(32) Valderrama, J. O. The State of the Cubic Equations of State. *Ind. Eng. Chem. Res.* **2003**, *42*, 1603−1618.

(33) Gross, J.; Sadowski, G. Perturbed-Chain SAFT: An equation of state based on a perturbation theory for chain molecules. *Ind. Eng. Chem. Res.* **2001**, *40*, 1244−1260.

(34) Frenkel, D.; Smit, B. *Understanding molecular simulation: from algorithms to applications*, 2nd ed.; Academic Press: San Diego, CA, 2002.

(35) Sun, R.; Lai, S.; Dubessy, J. Calculations of vapor-liquid equilibria of the H_2O-N_2 and H_2O-H_2 systems with improved SAFT-LJ EOS. *Fluid Phase Equilib.* **2015**, *390*, 23−33.

(36) Meyer, M.; Tebbe, U.; Piiper, J. Solubility of inert gases in dog blood and skeletal muscle. *Pfluegers Arch.* **1980**, *384*, 131−134.

(37) Gillespie, P. C.; Wilson, G. M. *Vapor-Liquid Equilibrium Data on Water-Substitue Gas Components*; Gas Processors Association, 1980; pp RR_41, pp 1−34; https://www.osti.gov/biblio/6782591 (accessed 17/7/2019).

(38) Kling, G.; Maurer, G. The solubility of hydrogen in water and in 2-aminoethanol at temperatures between 323 and 423 K and pressures up to 16 M Pa. *J. Chem. Thermodyn.* **1991**, *23*, 531−541.

(39) Devaney, W.; Berryman, J. M.; Kao, P.-L.; Eakin, B. *High Temperature V-L-E Measurements for Substitute Gas Components*; Gas Processors Association, 1978; pp 1−27.

(40) Jung, J. Loslichkeit von Kohlenmonoxid und Wasserstoff in Wasser zwisen 0 C und 300 C. Ph.D. Thesis, RWTH Aachen, 1962.

(41) Ipatev, V.; Teodorovich, V. Equilibrium compositions of vapor-gas mixtures over solutions. *Zh. Obshch. Khim.* **1934**, *4*, 395−399.

(42) Ugrozov, V. V. Equilibrium compositions of vapor-gas mixtures over solutions. *Russ. J. Phys. Chem.* **1996**, *70*, 1240−1241.

(43) Maslennikova, V. Y.; Goryunova, N.; Subbotina, L.; Tsiklis, D. The solubility of water in compressed hydrogen. *Russ. J. Phys. Chem.* **1976**, *50*, 240−243.

(44) Panagiotopoulos, A. Z. Molecular simulation of phase equilibria: simple, ionic and polymeric fluids. *Fluid Phase Equilib.* **1992**, *76*, 97−112.

(45) Panagiotopoulos, A. Z. Direct determination of fluid-Phase equilibria by simulation in the Gibbs ensemble - a Review. *Mol. Simul.* **1992**, *9*, 1−23.

(46) Panagiotopoulos, A. Z. Direct determination of phase coexistence properties of fluids by Monte Carlo simulation in a new ensemble. *Mol. Phys.* **1987**, *61*, 813−826.

(47) Recht, J.; Panagiotopoulos, A. Z. Finite-size effects and approach to criticality in Gibbs ensemble simulations. *Mol. Phys.* **1993**, *80*, 843−852.

(48) Siepmann, J. I.; McDonald, I. R.; Frenkel, D. Finite-size corrections to the chemical potential. *J. Phys.: Condens. Matter* **1992**, *4*, 679.

(49) Smit, B.; Frenkel, D. Calculation of the chemical potential in the Gibbs ensemble. *Mol. Phys.* **1989**, *68*, 951−958.

(50) Rahbari, A.; Poursaeidesfahani, A.; Torres-Knoop, A.; Dubbeldam, D.; Vlugt, T. J. H. Chemical potentials of water, methanol, carbon dioxide and hydrogen sulphide at low temperatures using continuous fractional component Gibbs ensemble Monte Carlo. *Mol. Simul.* **2018**, *44*, 405−414.

(51) Coskuner, O.; Deiters, U. K. Hydrophobic interactions by Monte Carlo simulations. *Z. Phys. Chem.* **2006**, *220*, 349−369.

(52) Shi, W.; Maginn, E. J. Continuous Fractional Component Monte Carlo: an adaptive biasing method for open system atomistic simulations. *J. Chem. Theory Comput.* **2007**, *3*, 1451−1463.

(53) Shi, W.; Maginn, E. J. Improvement in molecule exchange efficiency in Gibbs ensemble Monte Carlo: development and implementation of the continuous fractional component move. *J. Comput. Chem.* **2008**, *29*, 2520−2530.

(54) Poursaeidesfahani, A.; Torres-Knoop, A.; Dubbeldam, D.; Vlugt, T. J. H. Direct free energy calculation in the Continuous Fractional Component Gibbs ensemble. *J. Chem. Theory Comput.* **2016**, *12*, 1481−1490.

(55) Poursaeidesfahani, A.; Hens, R.; Rahbari, A.; Ramdin, M.; Dubbeldam, D.; Vlugt, T. J. H. Efficient application of Continuous Fractional Component Monte Carlo in the reaction ensemble. *J. Chem. Theory Comput.* **2017**, *13*, 4452−4466.

(56) Rahbari, A.; Hens, R.; Dubbeldam, D.; Vlugt, T. J. H. Improving the accuracy of computing chemical potentials in CFCMC simulations. *Mol. Phys.* 2019,

(57) Poursaeidesfahani, A.; Rahbari, A.; Torres-Knoop, A.; Dubbeldam, D.; Vlugt, T. J. H. Computation of thermodynamic properties in the continuous fractional component Monte Carlo Gibbs ensemble. *Mol. Simul.* **2017**, *43*, 189−195.

(58) Rahbari, A.; Hens, R.; Nikolaidis, I. K.; Poursaeidesfahani, A.; Ramdin, M.; Economou, I. G.; Moultos, O. A.; Dubbeldam, D.; Vlugt, T. J. H. Computation of partial molar properties using continuous fractional component Monte Carlo. *Mol. Phys.* **2018**, *116*, 3331−3344.

(59) Torres-Knoop, A.; Burtch, N. C.; Poursaeidesfahani, A.; Balaji, S. P.; Kools, R.; Smit, F. X.; Walton, K. S.; Vlugt, T. J. H.; Dubbeldam, D. Optimization of Particle Transfers in the Gibbs Ensemble for Systems with Strong and Directional Interactions Using CBMC, CFCMC, and CB/CFCMC. *J. Phys. Chem. C* **2016**, *120*, 9148−9159.

(60) Rahbari, A.; Hens, R.; Jamali, S. H.; Ramdin, M.; Dubbeldam, D.; Vlugt, T. J. H. Effect of truncating electrostatic interactions on predicting thermodynamic properties of water-methanol systems. *Mol. Simul.* **2019**, *45*, 336−350.

(61) Dubbeldam, D.; Calero, S.; Ellis, D. E.; Snurr, R. Q. RASPA: molecular simulation software for adsorption and diffusion in flexible nanoporous materials. *Mol. Simul.* **2016**, *42*, 81−101.

(62) Dubbeldam, D.; Torres-Knoop, A.; Walton, K. S. On the inner workings of Monte Carlo codes. *Mol. Simul.* **2013**, *39*, 1253−1292.

(63) Allen, M. P.; Tildesley, D. J. *Computer simulation of liquids*, 2nd ed.; Oxford University Press: Oxford, United Kingdom, 2017.

(64) Klimovich, P. V.; Shirts, M. R.; Mobley, D. L. Guidelines for the analysis of free energy calculations. *J. Comput.-Aided Mol. Des.* **2015**, *29*, 397−411.

(65) Naden, L. N.; Pham, T. T.; Shirts, M. R. Linear basis function approach to efficient alchemical free energy calculations. 1. Removal of uncharged atomic sites. *J. Chem. Theory Comput.* **2014**, *10*, 1128−1149.

(66) Naden, L. N.; Shirts, M. R. Linear basis function approach to efficient alchemical free energy calculations. 2. Inserting and deleting particles with Coulombic interactions. *J. Chem. Theory Comput.* **2015**, *11*, 2536−2549.

(67) Shirts, M. R.; Pande, V. S. Solvation free energies of amino acid side chain analogs for common molecular mechanics water models. *J. Chem. Phys.* **2005**, *122*, 134508.

(68) Shirts, M. R.; Pitera, J. W.; Swope, W. C.; Pande, V. S. Extremely precise free energy calculations of amino acid side chain analogs: Comparison of common molecular mechanics force fields for proteins. *J. Chem. Phys.* **2003**, *119*, 5740−5761.

(69) Shirts, M. R.; Mobley, D. L.; Chodera, J. D. In *Annual Reports in Computational Chemistry*; Spellmeyer, D., Wheeler, R., Eds.; Elsevier: United States, 2007; pp 41−59.

(70) Deeg, K. S.; Gutierrez-Sevillano, J. J.; Bueno-Perez, R.; Parra, J. B.; Ania, C. O.; Doblare, M.; Calero, S. Insights on the Molecular Mechanisms of Hydrogen Adsorption in Zeolites. *J. Phys. Chem. C* **2013**, *117*, 14374−14380.

(71) Sesé, L. M. Study of the Feynman-Hibbs effective potential against the path-integral formalism for Monte Carlo simulations of quantum many-body Lennard-Jones systems. *Mol. Phys.* **1994**, *81*, 1297−1312.

(72) Sesé, L. M. Feynman-Hibbs potentials and path integrals for quantum Lennard-Jones systems: Theory and Monte Carlo simulations. *Mol. Phys.* **1995**, *85*, 931−947.

(73) Izadi, S.; Anandakrishnan, R.; Onufriev, A. V. Building Water Models: a different approach. *J. Phys. Chem. Lett.* **2014**, *5*, 3863−3871.

(74) Vega, C.; Abascal, J. L. F.; Conde, M. M.; Aragones, J. L. What ice can teach us about water interactions: a critical comparison of the performance of different water models. *Faraday Discuss.* **2009**, *141*, 251−276.

(75) Lemmon, E. W.; Span, R. Short fundamental equations of state for 20 industrial fluids. *J. Chem. Eng. Data* **2006**, *51*, 785−850.

(76) Lemmon, E. W.; Huber, M. L.; McLinden, M. O. NIST reference fluid thermodynamic and transport properties−REFPROP. *NIST standard reference database* **2002**, *23*, v7.

(77) Buch, V. Path integral simulations of mixed para-D_2 and ortho-D_2 clusters: The orientational effects. *J. Chem. Phys.* **1994**, *100*, 7610−7629.

(78) Hirschfelder, C.; Curtiss, F.; Bird, R. B. *Molecular Theory of Gases and Liquids*; Wiley: New York, 1954.

(79) Köster, A.; Thol, M.; Vrabec, J. Molecular Models for the Hydrogen Age: Hydrogen, Nitrogen, Oxygen, Argon, and Water. *J. Chem. Eng. Data* **2018**, *63*, 305−320.

(80) Cracknell, R. F. Molecular simulation of hydrogen adsorption in graphitic nanofibres. *Phys. Chem. Chem. Phys.* **2001**, *3*, 2091−2097.

(81) Belof, J. L.; Stern, A. C.; Space, B. An accurate and transferable intermolecular diatomic hydrogen potential for condensed phase simulation. *J. Chem. Theory Comput.* **2008**, *4*, 1332−1337.

(82) Forrest, K. A.; Pham, T.; McLaughlin, K.; Belof, J. L.; Stern, A. C.; Zaworotko, M. J.; Space, B. Simulation of the mechanism of gas sorption in a metal-organic framework with open metal sites: molecular hydrogen in PCN-61. *J. Phys. Chem. C* **2012**, *116*, 15538−15549.

(83) Marx, D.; Nielaba, P. Path-integral Monte Carlo techniques for rotational motion in two dimensions: Quenched, annealed, and no-spin quantum-statistical averages. *Phys. Rev. A: At., Mol., Opt. Phys.* **1992**, *45*, 8968−8971.

(84) Camp, J.; Stavila, V.; Allendorf, M. D.; Prendergast, D.; Haranczyk, M. Critical factors in computational characterization of hydrogen storage in metal-organic frameworks. *J. Phys. Chem. C* **2018**, *122*, 18957−18967.

(85) Yang, Q.; Zhong, C. Molecular simulation of carbon dioxide/methane/hydrogen mixture adsorption in metal-organic frameworks. *J. Phys. Chem. B* **2006**, *110*, 17776−17783.

(86) Darkrim, F.; Levesque, D. Monte Carlo simulations of hydrogen adsorption in single-walled carbon nanotubes. *J. Chem. Phys.* **1998**, *109*, 4981−4984.

(87) Wagner, W.; Pruß, A. The IAPWS formulation 1995 for the thermodynamic properties of ordinary water substance for general and scientific use. *J. Phys. Chem. Ref. Data* **2002**, *31*, 387−535.

(88) Vega, C.; Abascal, J. L. F. Simulating water with rigid non-polarizable models: a general perspective. *Phys. Chem. Chem. Phys.* **2011**, *13*, 19663−19688.

(89) Abascal, J. L. F.; Vega, C. A general purpose model for the condensed phases of water: TIP4P/2005. *J. Chem. Phys.* **2005**, *123*, 234505.

(90) Tsimpanogiannis, I. N.; Moultos, O. A.; Franco, L. F. M.; de M. Spera, M. B.; Erdös, M.; Economou, I. G. Self-diffusion coefficient of bulk and confined water: a critical review of classical molecular simulation studies. *Mol. Simul.* **2019**, *45*, 425−453.

(91) Vega, C. Water: one molecule, two surfaces, one mistake. *Mol. Phys.* **2015**, *113*, 1145−1163.

(92) Bauer, B. A.; Patel, S. Properties of water along the liquid-vapor coexistence curve via molecular dynamics simulations using the polarizable TIP4P-QDP-LJ water model. *J. Chem. Phys.* **2009**, *131*, No. 084709.

(93) Jiang, H.; Moultos, O. A.; Economou, I. G.; Panagiotopoulos, A. Z. Hydrogen-bonding polarizable intermolecular potential model for water. *J. Phys. Chem. B* **2016**, *120*, 12358−12370.

(94) Chen, B.; Xing, J.; Siepmann, J. I. Development of polarizable water force fields for phase equilibrium calculations. *J. Phys. Chem. B* **2000**, *104*, 2391−2401.

(95) Yesylevskyy, S. O.; Schäfer, L. V.; Sengupta, D.; Marrink, S. J. Polarizable Water Model for the Coarse-Grained MARTINI Force Field. *PLoS Comput. Biol.* **2010**, *6*, 1−17.

(96) Gladich, I.; Roeselová, M. Comparison of selected polarizable and nonpolarizable water models in molecular dynamics simulations of ice I_h. *Phys. Chem. Chem. Phys.* **2012**, *14*, 11371−11385.

(97) Kunz, A.-P. E.; van Gunsteren, W. F. Development of a nonlinear classical polarization model for liquid water and aqueous solutions: COS/D. *J. Phys. Chem. A* **2009**, *113*, 11570−11579.

(98) Lamoureux, G.; MacKerell, A. D.; Roux, B. A simple polarizable model of water based on classical Drude oscillators. *J. Chem. Phys.* **2003**, *119*, 5185−5197.

(99) Lamoureux, G.; Harder, E.; Vorobyov, I. V.; Roux, B.; MacKerell, A. D. A polarizable model of water for molecular dynamics simulations of biomolecules. *Chem. Phys. Lett.* **2006**, *418*, 245−249.

(100) Ren, P.; Ponder, J. W. Polarizable atomic multipole water model for molecular mechanics simulation. *J. Phys. Chem. B* **2003**, *107*, 5933−5947.

(101) Laury, M. L.; Wang, L.-P.; Pande, V. S.; Head-Gordon, T.; Ponder, J. W. Revised parameters for the AMOEBA polarizable atomic multipole water model. *J. Phys. Chem. B* **2015**, *119*, 9423−9437.

(102) Jorgensen, W. L.; Chandrasekhar, J.; Madura, J. D.; Impey, R. W.; Klein, M. L. Comparison of simple potential functions for simulating liquid water. *J. Chem. Phys.* **1983**, *79*, 926−935.

(103) Jorgensen, W. L.; Chandrasekhar, J.; Madura, J. D.; Impey, R. W.; Klein, M. L. Comparison of simple potential functions for simulating liquid water. *J. Chem. Phys.* **1983**, *79*, 926−935.

(104) Mark, P.; Nilsson, L. Structure and dynamics of the TIP3P, SPC, and SPC/E water models at 298 K. *J. Phys. Chem. A* **2001**, *105*, 9954−9960.

(105) Berendsen, H. J. C.; Grigera, J. R.; Straatsma, T. P. The missing term in effective pair potentials. *J. Phys. Chem.* **1987**, *91*, 6269−6271.

(106) Horn, H. W.; Swope, W. C.; Pitera, J. W.; Madura, J. D.; Dick, T. J.; Hura, G. L.; Head-Gordon, T. Development of an improved four-site water model for biomolecular simulations: TIP4P-Ew. *J. Chem. Phys.* **2004**, *120*, 9665−9678.

(107) Rick, S. W. A reoptimization of the five-site water potential (TIP5P) for use with Ewald sums. *J. Chem. Phys.* **2004**, *120*, 6085−6093.

(108) Peng, D.-Y.; Robinson, D. B. A new two-constant equation of state. *Ind. Eng. Chem. Fundam.* **1976**, *15*, 59−64.

(109) Soave, G. Equilibrium constants from a modified Redlich-Kwong equation of state. *Chem. Eng. Sci.* **1972**, *27*, 1197−1203.

(110) Twu, C. H.; Coon, J. E.; Bluck, D. Comparison of the Peng-Robinson and Soave- Redlich-Kwong equations of state using a new zero-pressure-based mixing Rule for the prediction of high-pressure and high-temperature phase equilibria. *Ind. Eng. Chem. Res.* **1998**, *37*, 1580−1585.

(111) Péneloux, A.; Rauzy, E.; Fréze, R. A consistent correction for Redlich-Kwong-Soave volumes. *Fluid Phase Equilib.* **1982**, *8*, 7−23.

(112) Lin, C.-T.; Daubert, T. E. Estimation of partial molar volume and fugacity coefficient of components in mixtures from the soave and Peng-Robinson equations of state. *Ind. Eng. Chem. Process Des. Dev.* **1980**, *19*, 51−59.

(113) Leachman, J. W.; Jacobsen, R. T.; Penoncello, S.; Lemmon, E. W. Fundamental equations of state for parahydrogen, normal hydrogen, and orthohydrogen. *J. Phys. Chem. Ref. Data* **2009**, *38*, 721−748.

(114) Horn, H. W.; Swope, W. C.; Pitera, J. W.; Madura, J. D.; Dick, T. J.; Hura, G. L.; Head-Gordon, T. Development of an improved four-site water model for biomolecular simulations: TIP4P-EW. *J. Chem. Phys.* **2004**, *120*, 9665−9678.

(115) Mahoney, M. W.; Jorgensen, W. L. A five-site model for liquid water and the reproduction of the density anomaly by rigid,

nonpolarizable potential functions. *J. Chem. Phys.* **2000**, *112*, 8910−8922.

(116) Wilhelm, E.; Waghorne, E.; Hefter, G.; Hummel, W.; Maurer, G.; Rebelo, L. P. N.; da Ponte, M. N.; Battino, R.; Clever, L.; van Hook, A.; Domanska-Zelazna, U.; Tomkins, R. P. T.; Richon, D.; de Stafani, V.; Coquelet, C.; Costa Gomes, M.; Siepmann, J. I.; Anderson, K. E.; Eckert, F.; Grolier, J.-P.; Boyer, S.; Salminen, J.; Dohrn, R.; Leiberich, R.; Fele Zilnik, L.; Fages, J.; Macedo, M. E.; Gmehling, J.; Brennecke, J.; Cordes, W.; Prausnitz, J.; Goodwin, A. R.; Marsh, K.; Peters, C. J.; Voigt, W.; Koenigsberger, E.; May, P.; Kamps, A. P.-S.; Shariati, A.; Raeissi, S.; Padua, A. A. H.; Sauceau, M.; Pinho, S. P. P.; Kaskiala, T.; Kobylin, P. In *Developments and Applications in Solubility*; Letcher, T. M., Ed.; The Royal Society of Chemistry, 2007.